Aerospace Science and Technology 106 (2020) 106198

Contents lists available at ScienceDirect

Aerospace Science and Technology

www.elsevier.com/locate/aescte

Low-thrust planar transfer for co-planar low Earth orbit satellites considering self-induced collision avoidance

S. Huang *, C. Colombo, F. Bernelli-Zazzera

Department of Aerospace Science and Technology, Politecnico di Milano, Milano, MI, 20156, Italy

ARTICLE INFO

Article history:
Received 10 December 2019
Received in revised form 14 April 2020
Accepted 6 September 2020
Available online 11 September 2020
Communicated by Tsourdos Antonios

ABSTRACT

This paper deals with the planar transfer problems (orbit raising and de-orbiting) for co-planar satellites with low-thrust propulsion, taking the self-induced collision avoidance into consideration at the mission design stage. A Blended Error-Correction steering law, with which the thrust direction changes in a self-adaptive way, is developed by blending two types of efficient steering laws and offsetting the errors of the instantaneous orbit with respect to the target orbit. The semi-analytical solutions for orbital elements, which reduce the computational load of propagating long-duration trajectories, are derived by computing the analytical incremental changes in orbital elements after every revolution with an orbital averaging technique. Based on the analytical Blended Error-Correction steering law and semi-analytical solutions, transfers can be computed quickly for any starting times. Finally, the self-induced collision, which is modeled by miss distance, is avoided by scheduling properly the timing to start transfer for every satellite.

1. Introduction

In the recent past, several companies, such as OneWeb [1] and SpaceX [2], have disclosed their plan to build up large constellations consisting of hundreds to thousands of satellites in Low Earth Orbit (LEO). The purpose is to provide high-speed telecommunications services to the global Earth, even the most rural areas. With the sheer-sized constellations injected to the already congested LEO regime, collision is one of the most challenging problems for the designers and operators given the catastrophic damage it may result in. Therefore, the consideration for collision avoidance must cover the entire mission including the transfer phases of orbit raising and de-orbiting [3,4].

Low-thrust propulsion, which can provide high exhaust velocity and hence reduce the fuel costs, have been considered for various space missions, such as orbit transfers, station keeping, rendezvous, and also proximate pursuit-evasion [5]. Two types of methods have been widely used for low-thrust trajectory design – indirect methods and direct methods. Indirect methods address a two-point boundary value problem with the shooting method. However, the optimal solutions are difficult to obtain due to the small convergence radius and sensitivity to the initial guess. Direct methods transform the optimal control problem into a nonlinear programming problem and have a relatively larger convergence radius. Betts [6] proposed a sequential quadratic programming method to cope with a 578-revolution Earth-orbit transfer containing 416123 variables. Kluever and Oleson [7] blended the three extremal control laws and then used the direct method to optimize the weight of each control law. Gao [8] employed three steering laws over different orbital arcs in every revolution and then employed the direct method to optimize the length of orbital arcs. However, in the direct method, the number of optimization variables is usually large and thus not computationally efficient. To reduce the computational load, Fan et al. [9] conducted a fast design of low-thrust trajectory by using finite Fourier series which could provide suitable approximations and lead to accurate trajectory optimizations for multi-asteroid exploration. Considering that orbit transfers of multiple satellites in large constellations require a trajectory to be designed rapidly for every satellite, it would be preferable to develop an analytical control law that can be applied directly to every satellite. Ruggiero et al. [10] proposed closed-loop guidance laws by simultaneously offsetting the instantaneous errors in orbital elements. Zhang et al. [11] developed two analytical control laws for solving minimum-time and minimum-fuel low-thrust transfers to geosynchronous orbits by optimizing the objective functions based on the strategies they proposed.

* Corresponding author.
E-mail addresses: simeng.huang@polimi.it (S. Huang), camilla.colombo@polimi.it (C. Colombo), franco.bernelli@polimi.it (F. Bernelli-Zazzera).

https://doi.org/10.1016/j.ast.2020.106198

Nomenclature

g_0	Earth's gravitational acceleration at the sea-level, km/s^2	η	thrust engine efficiency, %
μ	Earth's gravitational constant, km^3/s^2	I_{sp}	thrust engine specific impulse, s
R_E	Earth's radius, km	c_t	weight for the tangential thrust
a	semi-major axis, km	c_i	weight for the inertial thrust
e	eccentricity	k_a	instantaneous error in semi-major axis
ω	argument of perigee, rad	k_e	instantaneous error in eccentricity
f	true anomaly, rad	d_{miss}	satellite-pair miss distance, km
E	eccentric anomaly, rad	D_{miss}	constellation miss distance, km
ϕ	true latitude, rad	t_{total}	total transfer time, s
γ	flight path angle, rad	Δt_0^{safe}	critical transfer starting time difference ensuring the safe transfer, s
n	mean motion, rad/s	$\Delta t_0^{\text{safest}}$	critical transfer starting time difference ensuring the safest transfer, s
r	orbital radius, km	N	number of satellites
u	magnitude of the low-thrust acceleration, km/s^2	Subscripts	
u_r	radial component of the low-thrust acceleration, km/s^2	0	initial orbital element
u_θ	transversal component of the low-thrust acceleration, km/s^2	f	final orbital element
α	pitch angle, rad	d	desired target orbital element
m	spacecraft mass, kg	t	tangential thrust
P	thrust engine power, W	i	inertial thrust

For satellite constellations, the low-thrust transfer is usually a coupled problem of trajectory design and constellation performance optimization. For example, Di Carlo et al. [12] used low-thrust combined with J_2 secular effects to deploy a constellation of 27 satellites in Medium Earth Orbit; then the problem was formulated as a multi-objective optimization problem to find the optimal deployment strategy by taking into account the change in velocity, launch sequence, and monetary pay-off. In our case, the constellation performance to be considered is the self-induced collision. For large constellations, due to the fact that multiple satellites will maneuver at the same time, the problem of self-induced collision – the collision caused only by the satellites from the constellation – will arise. Some studies have been conducted, in which the collision risk is modeled and computed to analyze the impacts of large constellations on the space debris environment [13–15]. Lee et al. [16] addressed the collision problem by conducting sub-optimal control for cooperative collision-free transfers of multiple satellites using continuous thrust, and the results can be used in real-time by large constellations.

Aiming at avoiding the self-induced collision for large constellations at the mission design stage, this work deals with the orbital transfer problems (orbit raising and de-orbiting) by combining the low-thrust trajectory design with the consideration for self-induced collision avoidance. As a preliminary study, this paper focuses on planar transfer for one orbital plane of the constellation, i.e. coplanar satellites. Inspired by the works in Refs. [7,8,10], this paper develops a Blended Error-Correction (BEC) steering law by blending two types of steering laws – tangential thrust and inertial thrust – and offsetting the errors of the instantaneous orbit with respect to the target orbit. With the BEC steering law, the thrust direction can change efficiently in a self-adaptive way. Besides, since the control law is analytical, it can be applied directly to every satellite without need for offline design. To further reduce the computational load of propagating long-duration trajectories, an orbital averaging technique is used by computing the analytical incremental changes in orbital elements after every revolution, through which two sets of semi-analytical solutions can be derived for orbit raising and de-orbiting missions. Based on the analytical BEC steering law and semi-analytical solutions, transfers from any starting times can be computed quickly for any satellites, making it possible to evaluate the miss distance, which is the minimum relative distance among satellites, for a transfer mission. This paper adopts the miss distance as the criterion to assess the self-induced collision risk; the larger the miss distance, the lower the collision risk. By scheduling properly the timing to start transfer for every satellites, the self-induced collision can be avoided.

Note that the scope of this study is only the propulsive phase. For orbit raising, it is the phase from the parking orbit to the final orbit at the nominal altitude, while excluding the final phasing angle adjustment. For de-orbiting, it is the active disposal phase, from the initial orbit to the re-entry perigee under which the atmospheric drag will lead the spacecraft to natural re-entry. Within this scope, the atmospheric drag can be neglected compared with the effects of low-thrust and Earth's gravity, and the self-induced collision is discussed between the active satellites composing the constellation.

The remaining of this paper is organized as follows. Sec. 2 introduces the dynamical model. Sec. 3 and 4 obtain the BEC steering law and semi-analytical solutions for orbital elements, respectively. Sec. 5 addresses the problem of self-induced collision, in which the transfer starting times are scheduled for orbit raising and de-orbiting missions, respectively.

2. Dynamical model

This paper addresses the problem of planar transfer, so the thrust acceleration vector lies within the orbital plane and the orbital elements to be studied are semi-major axis, eccentricity, argument of perigee, and true/eccentric anomaly. The rates of change of the orbital elements due to low-thrust are given by Gauss' equations [17]:

$$\frac{\mathrm{d}a}{\mathrm{d}t} = \frac{2a^2}{h}\left(e\sin f u_r + \frac{p}{r}u_\theta\right) \tag{1}$$

$$\frac{\mathrm{d}e}{\mathrm{d}t} = \frac{1}{h}\left(p\sin f u_r + \left((p+r)\cos f + re\right)u_\theta\right) \tag{2}$$

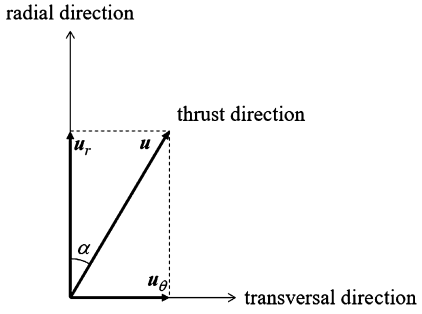

Fig. 1. Definition of the pitch angle.

$$\frac{\mathrm{d}\omega}{\mathrm{d}t} = \frac{1}{he}\left(-p\cos f\, u_r + (p+r)\sin f\, u_\theta\right) \tag{3}$$

$$\frac{\mathrm{d}E}{\mathrm{d}t} = \frac{na}{r} + \frac{1}{nae}\left(\left(\cos f - e\right)u_r - \left(1+\frac{r}{a}\right)\sin f\, u_\theta\right) \tag{4}$$

where, u_r and u_θ are the radial and transversal component of the thrust acceleration vector, respectively, a is the semi-major axis, e is the eccentricity, ω is the argument of perigee, E is the eccentric anomaly, f is the true anomaly, $r = a\left(1 - e\cos E\right)$ is the orbit radius, $p = a\left(1 - e^2\right)$ is the semi-latus rectum, $h = (\mu p)^{1/2}$ is the angular momentum with μ being the Earth's gravitational constant, $n = (\mu/a^3)^{1/2}$ is the mean motion. Because the thrust acceleration is much smaller (usually $\lesssim 10^{-6}$ km/s^2) than the Earth's gravitational acceleration ($>10^{-4}$ km/s^2), the rate of change of the eccentric anomaly can be approximated as

$$\frac{\mathrm{d}E}{\mathrm{d}t} \approx \frac{na}{r} \tag{5}$$

The relation between the true and eccentric anomaly is given by [17]

$$\cos f = \frac{\cos E - e}{1 - e\cos E}, \qquad \sin f = \frac{\sin E\sqrt{1-e^2}}{1 - e\cos E} \tag{6}$$

Then dividing Eqs. (1)–(3) by Eq. (5) and substituting Eq. (6), after some manipulations, the rate of change of the orbital elements with respect to the eccentric anomaly due to low-thrust can be obtained [18]

$$\frac{\mathrm{d}a}{\mathrm{d}E} = \frac{2a^3}{\mu}\left(e\sin E u_r + \sqrt{1-e^2}u_\theta\right) \tag{7}$$

$$\frac{\mathrm{d}e}{\mathrm{d}E} = \frac{a^2}{\mu}\left(\left(1-e^2\right)\sin E u_r + \sqrt{1-e^2}\left(2\cos E - e - e\cos^2 E\right)u_\theta\right) \tag{8}$$

$$\frac{\mathrm{d}\omega}{\mathrm{d}E} = \frac{a^2}{\mu e}\left(\sqrt{1-e^2}\left(e - \cos E\right)u_r + \left(2 - e^2 - e\cos E\right)\sin E u_\theta\right) \tag{9}$$

The averaged rates of change of the orbital elements due to J_2 perturbations are given by [17]

$$\frac{\mathrm{d}\bar{a}}{\mathrm{d}t} = \frac{\mathrm{d}\bar{e}}{\mathrm{d}t} = 0 \tag{10}$$

$$\frac{\mathrm{d}\bar{\omega}}{\mathrm{d}t} = \frac{3}{4}J_2\left(\frac{R_E}{p}\right)^2 n\left(5\cos^2 i - 1\right) \tag{11}$$

where the overbar represents the average orbital elements due to J_2 perturbations, R_E is the Earth's radius, and i is the inclination, which is different than zero and constant in this study. It has to be noticed that, due to the Earth's oblateness, the right ascension of the ascending node (RAAN) will change. During the transfer, different satellites are at the same inclination but at different altitude with different eccentricity, and they will be affected by a different RAAN shift rate. However, as this paper are focusing on the analysis of the planar behavior, in Sec. 5, the RAAN drifting will not be taken into account in the calculation of miss distance but will be verified and analyzed a posteriori.

3. Steering law design

Eqs. (7)–(9) will be integrated to evaluate the variations of the orbital elements over one revolution by using an orbital averaging technique in the next section; prior to this, the steering law should firstly be defined. Steering law is the time history of thrust direction which is described by the pitch angle α for planar transfer. In this work, the pitch angle is defined as the angle between the thrust direction and the radial direction, as shown in Fig. 1.

The radial and transversal component of the thrust acceleration vector are given by

$$u_r = u\cos\alpha, \qquad u_\theta = u\sin\alpha \tag{12}$$

where u is the magnitude of the thrust acceleration vector, given by

$$u = \frac{2\eta P}{m g_0 I_{sp}} \tag{13}$$

with m being the spacecraft mass, P being the power, η being the efficiency, I_{sp} being the specific impulse, and g_0 being the Earth's gravitational acceleration at the sea-level. The rate of change of the spacecraft mass is governed by

$$\frac{\mathrm{d}m}{\mathrm{d}t} = -m\frac{u}{g_0 I_{sp}} \tag{14}$$

Two steering laws – tangential thrust and inertial thrust – are used in this paper, for the following reasons: (1) tangential and inertial thrust are the local optimal and near optimal steering law to change the semi-major axis and eccentricity, respectively [8]; (2) the dynamical model by using these two steering laws is in simple form and hence it will allow to obtain the semi-analytical solutions. By blending these two steering laws and assigning a weight, which is given based on the error of the instantaneous orbit with respect to the target orbit, to each of them, an analytical Blended Error-Correction control law can be obtained.

3.1. Tangential thrust

Tangential thrust is the local optimal steering law to change the semi-major axis. The thrust direction aligns with the velocity direction. If the pitch angle is set to $\alpha = \gamma$, where γ is the flight path angle between the thrust and radial direction, then the thrust direction is along the velocity direction and the semi-major axis will be increased in the most efficient way. If the pitch angle is set to $\alpha = \gamma + \pi$, then the thrust direction is opposite to the velocity direction and the semi-major axis will be decreased in the most efficient way.

According to the relation between the flight path angle and the eccentric anomaly [17], the steering laws to increase and decrease the semi-major axis are respectively given by

$$\cos\alpha = \cos\gamma = \frac{e\sin E}{\sqrt{1-e^2\cos^2 E}}, \qquad \sin\alpha = \sin\gamma = \frac{\sqrt{1-e^2}}{\sqrt{1-e^2\cos^2 E}} \tag{15}$$

$$\cos\alpha = \cos(\gamma+\pi) = -\frac{e\sin E}{\sqrt{1-e^2\cos^2 E}}, \qquad \sin\alpha = \sin(\gamma+\pi) = -\frac{\sqrt{1-e^2}}{\sqrt{1-e^2\cos^2 E}} \tag{16}$$

Substituting Eqs. (12), (15) and (16) into Eqs. (7)–(9), the rates of change of the orbital elements with respect to the eccentric anomaly due to tangential thrust can be obtained:

$$\frac{\mathrm{d}a}{\mathrm{d}E} = \pm u\frac{2a^3}{\mu}\sqrt{1-e^2\cos^2 E} \tag{17}$$

$$\frac{\mathrm{d}e}{\mathrm{d}E} = \pm u\frac{2a^2\left(1-e^2\right)}{\mu}\sqrt{\frac{1-e\cos E}{1+e\cos E}}\cos E \tag{18}$$

$$\frac{\mathrm{d}\omega}{\mathrm{d}E} = \pm u\frac{2a^2\sqrt{1-e^2}}{\mu e}\sqrt{\frac{1-e\cos E}{1+e\cos E}}\sin E \tag{19}$$

where the sign + and – represents the cases of semi-major axis increase and decrease, respectively.

3.2. Inertial thrust

Inertial thrust is a near optimal steering law to change the eccentricity [8] [19]. The thrust direction is perpendicular to the periapsis radius. If the pitch angle is set to $\alpha = \pi/2 - f$, then the eccentricity will be increased. If the pitch angle is set to $\alpha = 3\pi/2 - f$, then the eccentricity will be decreased.

According to the relation between the true and eccentric anomaly [17], the steering laws to increase and decrease the eccentricity are respectively given by

$$\cos\alpha = \cos\left(\frac{\pi}{2}-f\right) = \frac{\sin E\sqrt{1-e^2}}{1-e\cos E}, \qquad \sin\alpha = \sin\left(\frac{\pi}{2}-f\right) = \frac{\cos E - e}{1-e\cos E} \tag{20}$$

$$\cos\alpha = \cos\left(\frac{3\pi}{2}-f\right) = -\frac{\sin E\sqrt{1-e^2}}{1-e\cos E}, \qquad \sin\alpha = \sin\left(\frac{3\pi}{2}-f\right) = -\frac{\cos E - e}{1-e\cos E} \tag{21}$$

Substituting Eqs. (12), (20) and (21) into Eqs. (7)–(9), the rates of change of the orbital elements with respect to the eccentric anomaly due to inertial thrust can be obtained:

$$\frac{\mathrm{d}a}{\mathrm{d}E} = \pm u\frac{2a^3\sqrt{1-e^2}}{\mu}\cos E \tag{22}$$

$$\frac{\mathrm{d}e}{\mathrm{d}E} = \pm u\frac{a^2\sqrt{1-e^2}}{\mu}\left(\cos^2 E - 2e\cos E + 1\right) \tag{23}$$

$$\frac{\mathrm{d}\omega}{\mathrm{d}E} = \pm u\frac{a^2}{\mu e}(\cos E - e)\sin E \tag{24}$$

where the sign + and – represents the cases of eccentricity increase and decrease, respectively.

3.3. Blended error-correction (BEC) steering law

To simultaneously change the orbital elements (i.e. semi-major axis and eccentricity), the thrust acceleration vector is given in the form of

$$\boldsymbol{u} = c_t \mathbf{u}_t + c_i \boldsymbol{u}_i = u\left(c_t \hat{\boldsymbol{u}}_t + c_i \hat{\boldsymbol{u}}_i\right) \tag{25}$$

where, $\boldsymbol{u}_t$ and $\boldsymbol{u}_i$ are the tangential and inertial thrust acceleration vector with the magnitude equal to u, respectively, c_t and c_i are the weights for tangential and inertial thrust, respectively, and the hat symbol $\hat{\bullet}$ represents the unit vector of the generic variable $\bullet$.

As mentioned above, the tangential and inertial thrust are the local and near optimal way to change the semi-major axis and eccentricity, respectively. Therefore, c_t and c_i in this work are set to be proportional to the instantaneous errors in semi-major axis and eccentricity, respectively, so that the orbital elements can change in a self-adaptively efficient way. The instantaneous errors in semi-major axis and eccentricity, denoted by k_a and k_e, respectively, are defined by the means of [10]

$$k_a = (a_d - a) / |a_d - a_0|, \qquad k_e = (e_d - e) / |e_d - e_0| \tag{26}$$

where, a_d and e_d are the desired target semi-major axis and eccentricity, a_0 and e_0 are the initial semi-major axis and eccentricity, and the symbol $|\bullet|$ represents the absolute value of the generic variable $\bullet$. Note that Eq. (26) can eliminate the dimensional difference between the semi-major axis and the eccentricity, as the semi-major axis is on the order of 10^3–10^5, whereas the eccentricity is less than 1.

For the orbit raising mission, a_d and e_d are the orbital elements of the final orbit, while for the de-orbiting mission, a_d and e_d are set to satisfy

$$h_{pf} = a_d (1 - e_d) - R_E \tag{27}$$

where h_{pf} is the final perigee altitude below which the atmospheric drag will lead the spacecraft to natural re-entry. To lower the perigee as fast as possible, a_d and e_d in the de-orbiting mission are chosen as

$$a_d = h_{pf} + R_E, \qquad e_d = 1 \tag{28}$$

Because $\hat{\boldsymbol{u}}_t$ and $\hat{\boldsymbol{u}}_i$ are in different directions, a normalization procedure is needed to ensure that the magnitude of $(c_t \hat{\boldsymbol{u}}_t + c_i \hat{\boldsymbol{u}}_i)$ in Eq. (25) is one. By using the cosine law, the weights c_t and c_i can be obtained:

$$c_t = \frac{k_a}{\sqrt{k_a^2 + k_e^2 + 2|k_a||k_e|\cos(\alpha_t - \alpha_i)}}, \qquad c_i = \frac{k_e}{\sqrt{k_a^2 + k_e^2 + 2|k_a||k_e|\cos(\alpha_t - \alpha_i)}} \tag{29}$$

where α_t and α_i are the pitch angle of the tangential and inertial thrust, respectively, given by

$$\alpha_t = \begin{cases} \gamma, & \text{if } k_a \geq 0 \\ \gamma + \pi, & \text{if } k_a < 0 \end{cases} \tag{30}$$

$$\alpha_i = \begin{cases} \frac{1}{2}\pi - f, & \text{if } k_e \geq 0 \\ \frac{3}{2}\pi - f, & \text{if } k_e < 0 \end{cases} \tag{31}$$

According to the definitions of tangential and inertial thrust, the term $\cos(\alpha_t - \alpha_i)$ equals to

$$\begin{aligned} \cos(\alpha_t - \alpha_i) &= \operatorname{sign}(k_a)\operatorname{sign}(k_e)\sin(\gamma + f) \\ &= \operatorname{sign}(k_a)\operatorname{sign}(k_e)\frac{\sqrt{1-e^2}\cos E}{\sqrt{1-e^2\cos^2 E}} \end{aligned} \tag{32}$$

where the symbol $\operatorname{sign}(\bullet)$ is the sign of the generic variable $\bullet$.

Substituting Eq. (32) into Eq. (29), c_t and c_i are finally given as a function of the instantaneous errors k_a and k_e and the eccentric anomaly E:

$$\begin{aligned} c_t &= \frac{k_a}{\sqrt{k_a^2 + k_e^2 + 2k_a k_e \frac{\sqrt{1-e^2}\cos E}{\sqrt{1-e^2\cos^2 E}}}} \\ c_i &= \frac{k_e}{\sqrt{k_a^2 + k_e^2 + 2k_a k_e \frac{\sqrt{1-e^2}\cos E}{\sqrt{1-e^2\cos^2 E}}}} \end{aligned} \tag{33}$$

The proposed steering law is referred to as the Blended Error-Correction (BEC) steering law, the blend of tangential thrust and inertial thrust, based on the offsets in the instantaneous errors in semi-major axis and eccentricity, and hence enabling the thrust direction to self-adaptively adjust according to the deviation of the instantaneous orbit towards the desired target orbit. It should be noticed that the idea of correcting the orbital elements was proposed by Ruggiero [10]. The difference between the previous work and this paper is the strategy to change the eccentricity. In the previous work, the steering law to change the eccentricity is local optimal, which is more efficient than the inertial thrust but in such case it would be impossible to obtain the semi-analytical solutions for the orbital elements, unless more approximations are introduced to simplify the dynamical model.

By using the BEC steering law, the rates of change of the orbital elements with respect to the eccentric anomaly due to low-thrust are given by

$$\frac{\mathrm{d}\boldsymbol{x}}{\mathrm{d}E} = c_t \left(+\frac{\mathrm{d}\boldsymbol{x}}{\mathrm{d}E}\right)_t + c_i \left(+\frac{\mathrm{d}\boldsymbol{x}}{\mathrm{d}E}\right)_i \tag{34}$$

where, $\boldsymbol{x} = [a, e, \omega]^T$, $(+\mathrm{d}\boldsymbol{x}/\mathrm{d}E)_t$ and $(+\mathrm{d}\boldsymbol{x}/\mathrm{d}E)_i$ are given by Eqs. (17)–(19) and Eqs. (22)–(24), respectively, with the sign + representing that the signs of the equations are positive.

4. Semi-analytical solutions

It is of high importance in the present work to further speed up the computation process of low-thrust trajectories because we are dealing with multiple satellites with different initial conditions. To reduce the computational load, in this section, an orbital averaging technique will be used to derive two sets of semi-analytical solutions for orbit raising and de-orbiting missions, and the numerical validations will be conducted to prove the accuracy of the semi-analytical solutions.

Due to the fact that the magnitude of the low-thrust acceleration is very small, typically on the order of 10^{-4} g_0 or less [20], all orbital elements except the eccentric anomaly can be assumed constant in one revolution. Under such assumption, the variations in the orbital elements (semi-major axis, eccentricity, and argument of perigee) over one revolution can be evaluated by integrating Eq. (34) in the eccentric anomaly from 0 to 2π:

$$\int_0^{2\pi} \frac{\mathrm{d}\boldsymbol{x}}{\mathrm{d}E}\mathrm{d}E = \int_0^{2\pi} \left(c_t \left(+\frac{\mathrm{d}\boldsymbol{x}}{\mathrm{d}E}\right)_t + c_i \left(+\frac{\mathrm{d}\boldsymbol{x}}{\mathrm{d}E}\right)_i\right)\mathrm{d}E + \frac{2\pi}{n}\frac{\mathrm{d}\bar{\boldsymbol{x}}}{\mathrm{d}t} \tag{35}$$

where the second term on the right side is the averaged variations due to J_2 perturbations over one revolution. Being this a preliminary study, the Earth's shadow effect is not considered in this paper.

No analytical solutions exist for Eq. (35). Noticing that the eccentricity of LEO orbits is comparatively small ($\leq$0.1), in this paper we compute a Taylor expansion in power of the eccentricity for the inverse of the denominator of c_t and c_i up to $O(e^2)$.

4.1. Orbit raising

The orbit raising mission in this work is assumed to raise the satellites from the parking orbits to the final circular orbits at the nominal altitude, i.e., $e_f = 0$; the final phasing angle adjustment is excluded from this preliminary study. According to Eq. (26), the errors in semi-major axis and eccentricity are given by

$$k_a = \frac{\Delta a}{a_f - a_0}, \qquad k_e = -\frac{e}{e_0} \tag{36}$$

where $\Delta a = a_f - a$.

Then substituting Eq. (36) into Eq. (33) and carrying out the expansion, c_t and c_i can be approximated as

$$c_t \approx R, \qquad c_i \approx -\frac{a_f - a_0}{\Delta a e_0} eR \tag{37}$$

where R is a binomial in the eccentricity, given by

$$R = 1 + \frac{a_f - a_0}{\Delta a e_0}\cos E e + \left(\frac{a_f - a_0}{\Delta a e_0}\right)^2 \frac{3\cos^2 E - 1}{2} e^2 \tag{38}$$

Substituting Eq. (37) into Eq. (34), and then carrying out the integration in E from 0 to 2π, after some manipulations, the variations in the orbital elements over one revolution can be derived:

$$\Delta a_{\mathrm{rev}} = \frac{4\pi a^3}{\mu}\left(1 - \frac{\left(a_f - a_0\right)^2 + \Delta a^2 e_0^2}{4\Delta a^2 e_0^2} e^2\right) u \tag{39}$$

$$\Delta e_{\mathrm{rev}} = -\frac{\pi a^2}{\mu}\frac{a_f - a_0 + 2\Delta a e_0}{\Delta a e_0} eu \tag{40}$$

$$\Delta \omega_{\mathrm{rev}} = -\frac{\pi a^2}{\mu}\frac{a_f - a_0}{\Delta a e_0} eu + \frac{3\pi R_E^2 J_2}{2a^2\left(1 - e^2\right)^2}\left(5\cos^2 i - 1\right) \tag{41}$$

4.2. De-orbiting

According to Eqs. (26)–(28), the errors in semi-major axis and eccentricity are given by

$$k_a = \frac{\Delta a}{a_0 - a_{pf}}, \qquad k_e = \Delta e \tag{42}$$

where, $a_{pf} = h_{pf} + R_E$, $\Delta a = a_{pf} - a$, and $\Delta e = 1 - e$.

Similar to orbit raising, substituting Eq. (42) into Eq. (33) and carrying out the expansion, c_t and c_i can be approximated as

$$c_t = \Delta a D, \qquad c_i = \left(a_0 - a_{pf}\right)\Delta e D \tag{43}$$

where D is a binomial in the eccentricity, given by

$$\begin{aligned} D = & \frac{D_0}{\left(\left(a_0 - a_{pf}\right)^2 + \Delta a^2 + 2\left(a_0 - a_{pf}\right)\Delta a \cos E\right)^{1/2}} \\ & + \frac{D_1}{\left(\left(a_0 - a_{pf}\right)^2 + \Delta a^2 + 2\left(a_0 - a_{pf}\right)\Delta a \cos E\right)^{3/2}} e \\ & + \frac{D_2}{\left(\left(a_0 - a_{pf}\right)^2 + \Delta a^2 + 2\left(a_0 - a_{pf}\right)\Delta a \cos E\right)^{5/2}} e^2 \end{aligned} \tag{44}$$

with D_0, D_1 and D_2 being

$$\begin{aligned} D_0 &= 1 \\ D_1 &= \left(a_0 - a_{pf}\right)\left(\left(a_0 - a_{pf}\right) + \Delta a \cos E\right) \\ D_2 &= \frac{a_0 - a_{pf}}{4}\left(\begin{array}{c} \left(a_0 - a_{pf}\right)\left(4\left(a_0 - a_{pf}\right)^2 + 3\Delta a^2\right) + 2\left(5\left(a_0 - a_{pf}\right)^2 + \Delta a^2\right)\Delta a \cos E \\ +3\left(a_0 - a_{pf}\right)\Delta a^2 \cos 2E - 2\left(\left(a_0 - a_{pf}\right)^2 + \Delta a^2\right)\Delta a \cos 3E - 2\left(a_0 - a_{pf}\right)\Delta a^2 \cos 4E \end{array}\right) \end{aligned} \tag{45}$$

Substituting Eq. (43) into Eq. (34), and then carrying out the integration in E from 0 to 2π, after some manipulations, the variations in the orbital elements over one revolution can be derived:

$$\Delta a_{\text{rev}} = \frac{2a^3}{\mu}\left(\frac{1}{a_0 - a}\left(a_t^{elliF}\Delta a + a_i^{elliF}\sqrt{1-e^2}\Delta e\right) elliF + \left(a_0 - a\right)\left(a_t^{elliE}\Delta a + a_t^{elliF}\sqrt{1-e^2}\Delta e\right) elliE\right) u \tag{46}$$

$$\Delta e_{\text{rev}} = \frac{a^2\sqrt{1-e^2}}{\mu}\left(\begin{array}{c} \frac{1}{a_0 - a}\left(e_t^{elliF}\sqrt{1-e^2}\Delta a + e_i^{elliF}\left(a_0 - a_{pf}\right)\Delta e\right) elliF \\ +\left(a_0 - a\right)\left(e_t^{elliE}\sqrt{1-e^2}\Delta a + e_i^{elliE}\left(a_0 - a_{pf}\right)\Delta e\right) elliE \end{array}\right) u \tag{47}$$

$$\Delta\omega_{\text{rev}} = \frac{3\pi R_E^2 J_2}{2a^2\left(1-e^2\right)^2}\left(5\cos^2 i - 1\right) \tag{48}$$

where a_t^{elliF}, a_i^{elliF}, a_t^{elliE}, a_t^{elliF}, e_t^{elliF}, e_i^{elliF}, e_t^{elliE} and e_i^{elliE} are the binomials in the eccentricity, reported in Appendix A.

Eqs. (46) and (47) contain some elliptic integrals to be evaluated once per revolution:

$$elliF = EllipticF\left(\pi, \frac{4\left(a_0 - a_{pf}\right)\Delta a}{\left(\left(a_0 - a_{pf}\right) + \Delta a\right)^2}\right) \tag{49}$$

where

$$EllipticF\left(\phi, \lambda\right) = \int_0^{\phi} \frac{1}{\sqrt{1 - \lambda \sin^2\varphi}} \mathrm{d}\varphi \tag{50}$$

is the first kind of incomplete elliptic integral [17], and

$$elliE = EllipticE\left(\pi, \frac{4\left(a_0 - a_{pf}\right)\Delta a}{\left(\left(a_0 - a_{pf}\right) + \Delta a\right)^2}\right) \tag{51}$$

where

$$EllipticE\left(\phi, \lambda\right) = \int_0^{\phi} \sqrt{1 - \lambda \sin^2\varphi}\,\mathrm{d}\varphi \tag{52}$$

is the second kind of incomplete elliptic integral [17].

4.3. Numerical validations

To verify the accuracy of the semi-analytical solutions, a comparison is conducted between the full dynamics integration and the semi-analytical solutions. Table 1 gives the characteristics of a stationary plasma thruster (SPT) [21]. The mission conditions are presented in Table 2. Note that, for the full dynamics integration, the lower boundary for the eccentricity is set to 10^{-4} in order to avoid the singularity during the integration of the argument of perigee.

Fig. 2 to Fig. 4 present the time histories of the orbital elements obtained by the full dynamics integration and the semi-analytical solutions for both missions.

It can be seen from the figures that the semi-analytical solutions can eliminate the short period effects and give the averaged orbital elements. Fig. 2–Fig. 4 show good agreement between the full dynamics integration and semi-analytical solutions. Although there exists

Table 1
Thruster characteristics.

P, W	η, %	I_{sp}, s
150	39.23	1500

Table 2
Mission conditions.

Mission	Initial conditions							Final conditions
			e					
	m_0, kg	a_0, km	Full	Semi	i_0, deg	ω_0, deg	f_0, deg	
Orbit raising	120	$500 + R_E$	10^{-2}	10^{-2}	87.9	0	30	$a_f = (1200 + R_E)$ km, $e_f < 10^{-4}$
De-orbiting	120	$1200 + R_E$	10^{-4}	0	87.9	0	30	$h_{pf} = 300$ km

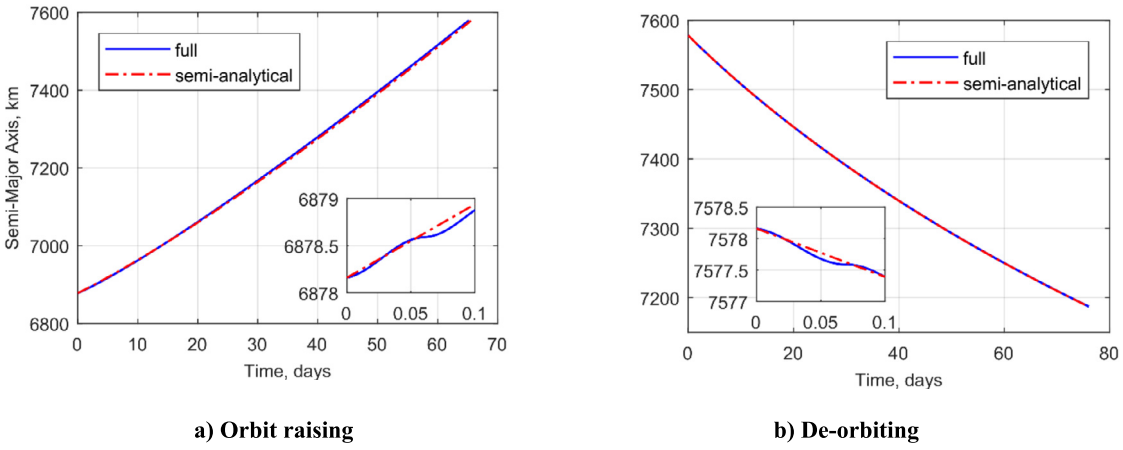

Fig. 2. Time history of the semi-major axis.

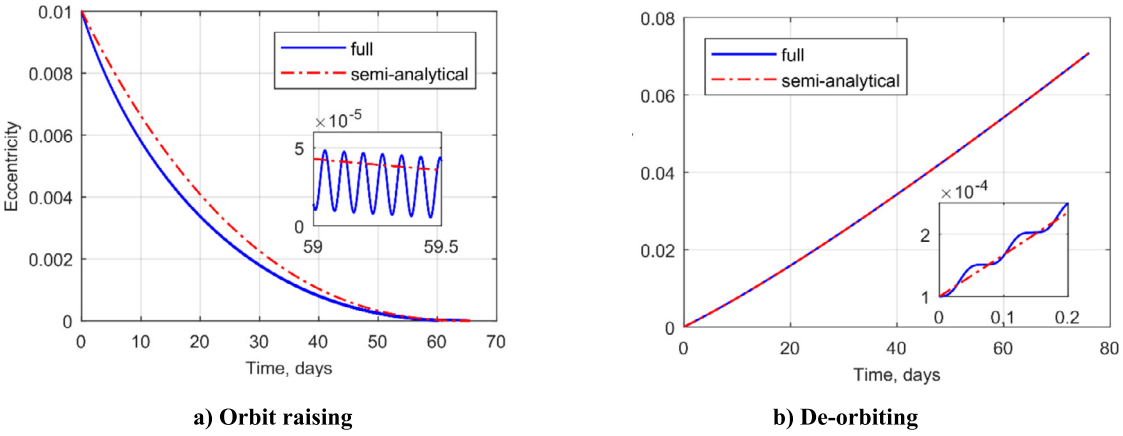

Fig. 3. Time history of the eccentricity.

a maximum error of less than 10^{-3} for the eccentricity in the orbit raising mission, which is introduced by the Taylor expansion, the semi-analytical results gradually convergence to the numerical integration and the final travel time is the same.

The results at the final time are presented in Table 3, again, showing good agreement.

The computation time of the full dynamics integration and the semi-analytical solutions are compared in Table 4, in which the relative and absolute tolerance for the full dynamics integration are 10^{-6} and 10^{-9}, respectively. It can be seen that the computation load can be drastically reduced by using the semi-analytical solutions.

5. Self-induced collision avoidance

With the analytical BEC steering law and semi-analytical solutions, the orbital transfers from any starting times can be computed in short time. The next step is to deal with the transfer problem for multiple satellites, in which the problem of self-induced collision arises. In this section, the self-induced collision risk is quantitatively evaluated by miss distance, and then the problem of self-induced collision is solved by scheduling properly the timing to start transfer for every satellite for orbit raising and de-orbiting missions.

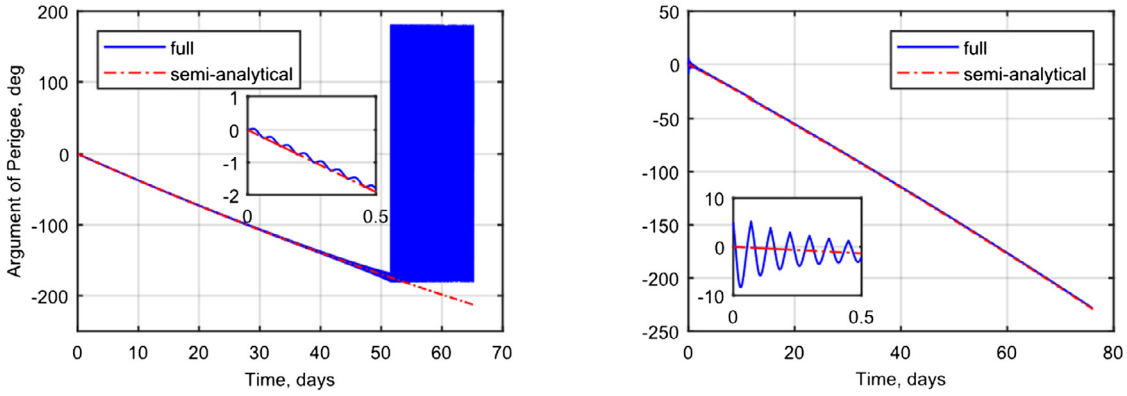

a) Orbit raising b) De-orbiting

Fig. 4. Time history of the argument of perigee.

Table 3
Results at the final time.

Mission	Full dynamics integration				Semi-analytical solutions			
	a_f, km	e_f	t_f, days	Δm_f, kg	a_f, km	e_f	t_f, days	Δm_f, kg
Orbit raising	7578.16	1.00×10^{-8}	65.20	3.06	7578.12	3.95×10^{-10}	65.55	3.08
De-orbiting	7187.32	7.08×10^{-2}	76.01	3.57	7186.82	7.10×10^{-2}	76.12	3.58

Table 4
Computation time.

Mission	Full dynamics integration	Semi-analytical solutions
Orbit raising	2.9739 s	0.0072 s
De-orbiting	3.1563 s	0.1706 s

5.1. Miss distance

The notion of miss distance in this paper is redefined in two levels.

The first level is the miss distance between two satellites, the minimum relative distance between two satellites over the entire transfer, referred to as the satellite-pair miss distance, and denoted by d_{miss}. The satellite-pair miss distance between satellites Ath and Bth is given by

$$d_{\text{miss}}^{AB} = \min \Delta r_{AB}(t), \qquad t \in \left[t_0^{AB}, t_f^{AB}\right] \tag{53}$$

where, $[t_0^{AB}, t_f^{AB}]$ is the time interval within which both the Ath and Bth satellite are in the propulsive transfer phase, t_0^{AB} and t_f^{AB} are given by

$$t_0^{AB} = \max\left\{t_0^A, t_0^B\right\}, \qquad t_f^{AB} = \min\left\{t_f^A, t_f^B\right\} \tag{54}$$

with t_0^A and t_f^A being the transfer starting and ending time of the Ath satellite, respectively, t_0^B and t_f^B being the transfer starting and ending time of the Bth satellite, respectively.

The second level is the miss distance of the constellation, the minimum satellite-pair miss distance of all satellite pairs from the constellation, referred to as the constellation miss distance, and denoted by D_{miss}. Supposing a constellation of N satellites, the constellation miss distance is given by

$$D_{\text{miss}} = \min_{1 \le A < B \le N} d_{\text{miss}}^{AB} \tag{55}$$

Through this assessment approach, the problem of avoiding the self-induced collision can be quantitatively transformed into increasing the constellation miss distance, which is equivalent to increasing the satellite-pair miss distance, whereas the satellite-pair miss distance is dependent on the relative motions of the satellites. Reminding that we are discussing planar transfer for coplanar satellites, the relative distance can be written as

$$\Delta r_{AB} = \sqrt{r_A^2 + r_B^2 - 2 r_A r_B \cos(\phi_A - \phi_B)} \tag{56}$$

where $\phi = \omega + f$, referred to in this paper as the true latitude.

Observing from Eq. (56), for given r_A and r_B, Δr_{AB} will reach its minimum, i.e., $\Delta r_{AB} = |r_A - r_B|$, when $\phi_A - \phi_B = 2k\pi$, where k is an integer. This implies that the satellite-pair miss distance is associated to the orbit radius difference when the latitude difference is a multiple integer of 2π. In this paper, such an event is referred to as latitude resonance.

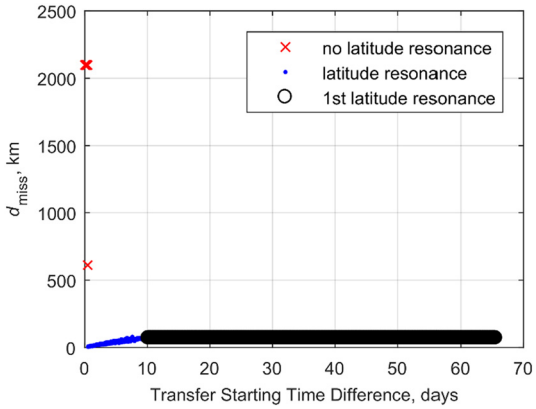

Fig. 5. Satellite-pair miss distance versus transfer starting time difference ($\Delta f_0 = 2\pi/20$ rad). (For interpretation of the colors in the figure(s), the reader is referred to the web version of this article.)

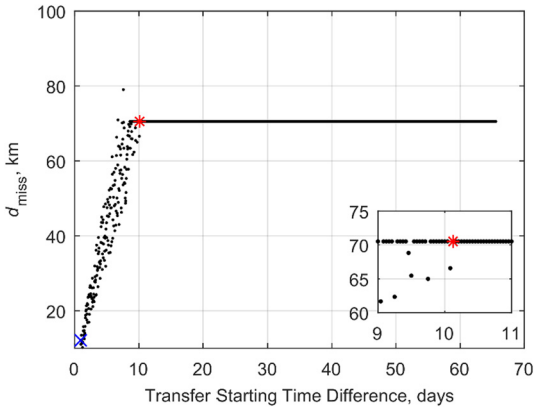

Fig. 6. Critical transfer starting time differences.

Since the transfer trajectories have been predefined for every satellite, the possible way to increase the miss distance is by properly scheduling the timing to start transfer for every satellite in the constellation. For no doubts the optimal solution for timing scheduling is to let all satellites start to transfer at the same timing, such that all satellites follow the same orbital path, and hence no collision will happen. However, in practical applications, the satellites usually cannot start to transfer at the same time. So, in this study, the transfer starting time is scheduled within the scope that the satellites do not start to transfer at the same time.

5.2. Transfer starting time scheduling for orbit raising mission

Fig. 5 shows the satellite-pair miss distance as a function of the transfer starting time difference for two satellites with the initial true anomaly difference of $2\pi/20$ rad. The mission conditions are given by Table 1 and Table 2. The red crosses indicate that the latitude resonance does not happen, i.e., the latitude difference never reaches 2π. The blue points and black circles indicate that the latitude resonance happens for one or multiple times. The difference is that, for the blue points, the miss distance equals to the relative distance at one of the latitude resonances, while for the black circles, the miss distance equals to the relative distance at the first latitude resonance. The detailed interpretation on these three cases is reported in Appendix B. Note that for the case that the latitude resonance does not happen, a small increase in the transfer starting time difference will lead to a sharp decline in the miss distance.

Fig. 6 shows in detail for the blue points and black circles of Fig. 5. In Fig. 6, all blue points and black circles from Fig. 5 are replaced with black points, and the x coordinates for the blue cross and red asterisk are equal to the critical transfer starting time differences Δt_0^{safe} and $\Delta t_0^{\text{safest}}$. Δt_0^{safe} denotes the safe time interval between two successive transfers. If the transfer starting time difference between two satellites is equal to or larger than Δt_0^{safe}, then the satellite-pair miss distance of these two satellites can be ensured higher than a given threshold (10 km for the present problem), and thus the transfers can be ensured safely enough. $\Delta t_0^{\text{safest}}$ stands for the safest time interval between two successive transfers. If the transfer starting time difference between two satellites is equal to or larger than $\Delta t_0^{\text{safest}}$, then the satellite-pair miss distance of these two satellites will increase to a constant number (70.5 km for the present problem), in which case the transfers can be ensured safest.

By checking the satellite-pair miss distance for the satellite pairs with different initial relative phases and identifying the critical transfer starting time difference, the mission designers can preliminarily estimate the self-induced collision risk and can have an idea about the safe time interval to do the next transfer.

Take as an example of 20 evenly spaced coplanar satellites. The mission conditions are given in Table 1 and Table 2. The critical transfer starting time difference is identified for the satellite pairs with different initial relative phases, presented in Table 5. The figures of the satellite-pair miss distance versus the transfer starting time difference are presented in Appendix C.

Table 5
Critical transfer starting time difference for different satellite pairs ($d_{\text{miss}} \geq 10$ km).

Δf_0, rad	Critical transfer starting time	
	Δt_0^{safe}, days	$\Delta t_0^{\text{safest}}$, days
$2\pi/20$	0.92	10.13
$4\pi/20$	0.92	12.42
$6\pi/20$	1.13	9.71
$8\pi/20$	1.04	11.58
$10\pi/20$	0.96	7.58
$12\pi/20$	0.96	10.13
$14\pi/20$	1.13	10.46
$16\pi/20$	1.25	7.58
$18\pi/20$	1.17	6.71
$20\pi/20$	1.21	9.42
$22\pi/20$	1.08	8.96
$24\pi/20$	1.25	8.54
$26\pi/20$	1.25	6.13
$28\pi/20$	1.29	7.38
$30\pi/20$	1.33	5.50
$32\pi/20$	1.54	5.46
$34\pi/20$	1.75	4.08
$36\pi/20$	1.83	3.83
$38\pi/20$	1.62	2.38

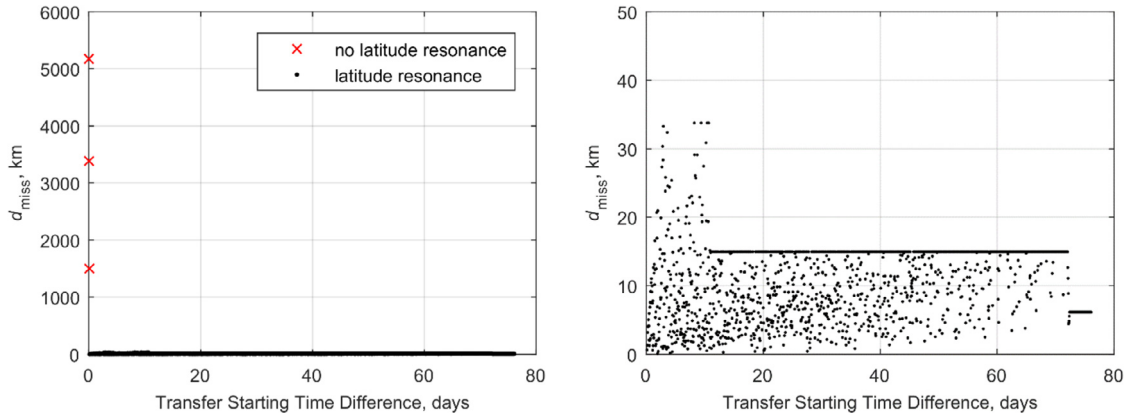

Fig. 7. Satellite-pair miss distance versus transfer starting time difference ($\Delta f_0 = 2\pi/8$ rad).

5.3. Transfer starting time scheduling for de-orbiting mission

Fig. 7 a) shows the satellite-pair miss distance as a function of the transfer starting time difference for two satellites with the initial true anomaly difference of $2\pi/8$ rad; the red crosses and black points indicate the cases that the latitude resonance does not happen and does happen, respectively. Fig. 7 b) is the zoom-in for Fig. 7 a) in terms of the cases that the latitude resonance happens. The mission conditions are given in Table 1 and Table 2. Same as Fig. 5, for the case that the latitude resonance does not happen, a small increase in the transfer starting time difference will lead to a sharp decline in the miss distance.

As shown in Fig. 7, for de-orbiting missions, the influence of the transfer starting time difference on the satellite-pair miss distance is not as clear as orbit raising missions (shown in Fig. 5 and Fig. 6). This is due to the fact that the de-orbiting trajectories are elliptical and hence the relative geometry of two de-orbiting trajectories are more complicated than the near-circular orbit raising trajectories. Therefore, we are not able to identify the critical transfer starting time difference for the de-orbiting missions in this preliminary study. Instead, the timing scheduling is done with the aid of multi-objective optimization.

The first objective is maximizing the constellation miss distance, i.e. minimizing the self-induced collision risk. The second objective is minimizing the total transfer time, from the first satellite starting the transfer to the last satellite finishing the transfer. This multi-objective optimization problem is modeled as

$$F_1 = -\min D_{\text{miss}} \tag{57}$$

$$F_2 = \min t_{\text{total}} \tag{58}$$

where, t_{total} is the total transfer time, given by

$$t_{\text{total}} = \max_{1 \leq B \leq N} \left\{ t_f^B \right\} - \min_{1 \leq A \leq N} \left\{ t_0^A \right\} \tag{59}$$

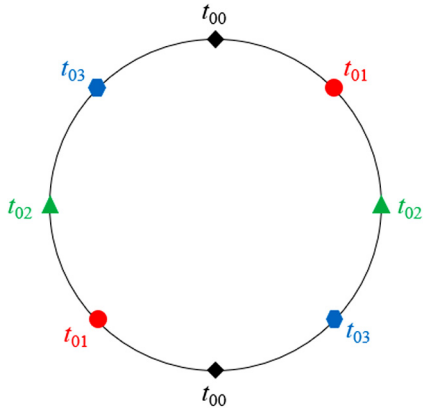

Fig. 8. De-orbiting strategy.

Table 6
Lower and upper bounds for the transfer starting time.

	Lower bounds			Upper bounds		
t_{00}, days	t_{01}, days	t_{02}, days	t_{03}, days	t_{01}, days	t_{02}, days	t_{03}, days
0	15	30	45	60	60	60

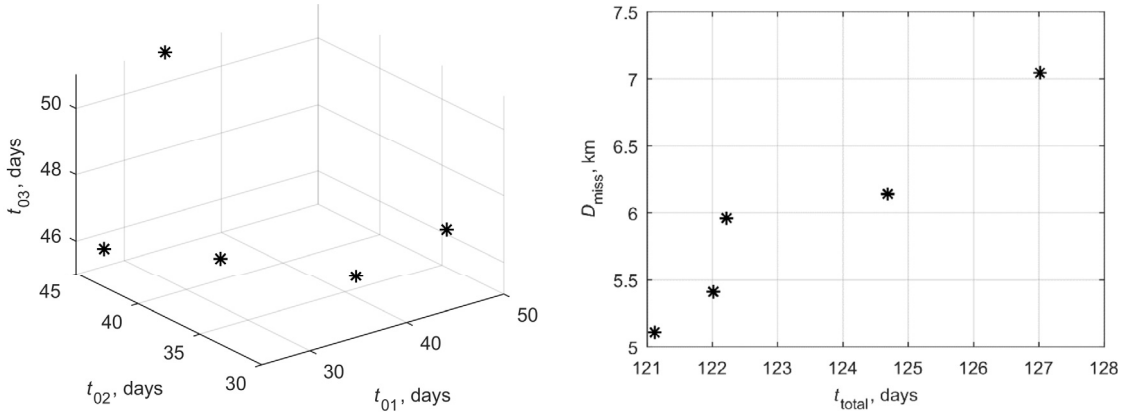

a) Transfer starting time.

b) Pareto front solutions – constellation miss distance versus total transfer time.

Fig. 9. Optimization results ($D_{\text{miss}} \geq 5$ km).

with N being the number of satellites in the constellation, t_0^A and t_f^B being the transfer starting and ending time of the Ath and Bth satellite, respectively.

Take as an example of 8 evenly spaced coplanar satellites. The mission conditions are given in Table 1 and Table 2. A de-orbiting strategy is also considered to remove the satellites in four groups, two satellites in each group, as shown in Fig. 8. In this figure, the satellites from different groups are represented by different colors; t_{00}–t_{03} indicate the transfer starting time of each group, and the satellites from the same group start to de-orbit at the same timing. The reason why to propose such a strategy is because the satellite-pair miss distance of the satellites in opposite positions is the maximum if they start to de-orbit at the same time.

A multi-objective global optimizer is used to search for the Pareto front solutions through a multi-agent-based search approach hybridized with a domain decomposition technique developed by Vasile [22]. The lower and upper bounds for the design variables, i.e. transfer starting time, are given in Table 6. Here, t_{00} is set to 0 and the minimum acceptable constellation miss distance is set to 5 km.

The optimization results are presented in Fig. 9 and Table 7, implying that a trade-off consideration for the constellation miss distance and the total transfer time is needed. Note that the constellation miss distance considering the RAAN shift due to J_2 perturbation is also verified a posteriori and presented in Table 7. In general, the constellation miss distance considering the RAAN shift satisfies the lower bound for D_{miss} ($\geq$5 km) and it is larger than the constellation miss distance that does not consider the RAAN shift, except for few cases. In further research, the RAAN shift should be included.

6. Conclusion

This paper dealt with the planar low-thrust orbit raising and de-orbiting problems for coplanar satellites and took the self-induced collision avoidance into consideration. A blended error-correction steering law, which could offset the instantaneous errors in orbital

Table 7
Optimization results ($D_{\text{miss}} \geq 5$ km).

t_{01}, days	t_{02}, days	t_{03}, days	t_{total}, days	D_{miss}, km	A posteriori D_{miss}, km
36.46	42.30	45	121.12	5.11	9.65
38.92	33.28	45.90	122.01	5.41	5.51
25.34	43.00	46.10	122.22	5.96	9.65
48.57	33.50	46.47	124.69	6.14	3.16
34.19	44.99	50.90	127.02	7.04	9.65

elements and adjust the thrust direction self-adaptively, was developed. Although not optimal, such steering law was analytical and thus could be applied directly to any satellites without need for offline design. Two sets of semi-analytical solutions are derived for the orbit raising and de-orbiting missions by using the orbital averaging technique, with which the computational time could be shortened a lot. The problem of reducing the self-induced collision risk was converted to increasing the miss distance, and it was solved by scheduling the transfer starting times for the satellites. For the orbit raising mission, the critical transfer starting time differences were identified, ensuring a large enough satellite-pair miss distance. For the de-orbiting mission, the optimal transfer starting times that could maximize the constellation miss distance and minimize the total transfer time were obtained by using the multi-objective optimization technique. Although the test transfers were solved for 20 satellites for orbit raising and 8 satellites for de-orbiting, the same approach could be followed to address a similar problem.

Two open points remain for the future research. The first one is the RAAN drifting due to J_2. This paper did not consider the RAAN drifting to focus on analyzing only the planar behavior. However, by checking a posteriori, in some cases the RAAN drifting did have negative influence on self-induced collision. The second problem to address is the transfer of non-planar satellites, i.e. multi-satellite and multi-plane. The two-layer-study methodology proposed in this paper, i.e. first designing trajectory and then solving collision avoidance, can be used to address a more general problem.

Declaration of competing interest

The authors declare that they have no known competing financial interests or personal relationships that could have appeared to influence the work reported in this paper.

Acknowledgements

The work performed for this paper has received funding from the European Research Council (ERC) under the European Union's Horizon 2020 research and innovation program as part of project COMPASS (Grant agreement No 679086).

Appendix A

The expressions of the coefficients that appear in Eqs. (46) and (47) are as follows.

$$a_t^{elliF} = 2 + e - \frac{3\left(a_0 - a_{pf}\right)^4 + 3\left(a_0 - a_{pf}\right)^2 \Delta a^2 + 3\Delta a^4}{2\left(a_0 - a_{pf}\right)^2 \Delta a^2} e^2 \tag{60}$$

$$a_i^{elliF} = -\frac{\left(a_0 - a_{pf}\right)^2 + \Delta a^2}{\Delta a} - \Delta a e + \frac{4\left(a_0 - a_{pf}\right)^6 + 6\left(a_0 - a_{pf}\right)^4 \Delta a^2 + \left(a_0 - a_{pf}\right)^2 \Delta a^4 + 4\Delta a^6}{5\left(a_0 - a_{pf}\right)^2 \Delta a^3} e^2 \tag{61}$$

$$a_t^{elliE} = \frac{1}{\left(a_0 - a_{pf}\right)^2 - \Delta a^2} e + \frac{3\left(a_0 - a_{pf}\right)^6 - 4\left(a_0 - a_{pf}\right)^2 \Delta a^4 + 3\Delta a^6}{2\left(a_0 - a_{pf}\right)^2 \Delta a^2 \left(\left(a_0 - a_{pf}\right)^2 - \Delta a^2\right)^2} e^2 \tag{62}$$

$$\begin{aligned} a_i^{elliE} = {} & \frac{1}{\Delta a} - \frac{\Delta a}{\left(a_0 - a_{pf}\right)^2 - \Delta a^2} e \\ & - \frac{4\left(a_0 - a_{pf}\right)^8 - 2\left(a_0 - a_{pf}\right)^6 \Delta a^2 + 6\left(a_0 - a_{pf}\right)^4 \Delta a^4 - 7\left(a_0 - a_{pf}\right)^2 \Delta a^6 + 4\Delta a^8}{5\left(a_0 - a_{pf}\right)^2 \Delta a^3 \left(\left(a_0 - a_{pf}\right)^2 - \Delta a^2\right)^2} e^2 \end{aligned} \tag{63}$$

$$\begin{aligned} e_t^{elliF} = {} & -\frac{\left(a_0 - a_{pf}\right)^2 + \Delta a^2}{\left(a_0 - a_{pf}\right) \Delta a} - \frac{\left(a_0 - a_{pf}\right)^4 + 4\left(a_0 - a_{pf}\right)^2 \Delta a^2 + 3\left(a_0 - a_{pf}\right) \Delta a^3 + \Delta a^4}{3\left(a_0 - a_{pf}\right)^2 \Delta a^2} e \\ & + \begin{pmatrix} \frac{22\left(a_0 - a_{pf}\right)^6 + 10\left(a_0 - a_{pf}\right)^5 \Delta a + 23\left(a_0 - a_{pf}\right)^4 \Delta a^2}{30\left(a_0 - a_{pf}\right)^3 \Delta a^3} \\ -\frac{20\left(a_0 - a_{pf}\right)^3 \Delta a^3 + 7\left(a_0 - a_{pf}\right)^2 \Delta a^4 + 20\left(a_0 - a_{pf}\right) \Delta a^5 - 22\Delta a^6}{30\left(a_0 - a_{pf}\right)^3 \Delta a^3} \end{pmatrix} e^2 \end{aligned} \tag{64}$$

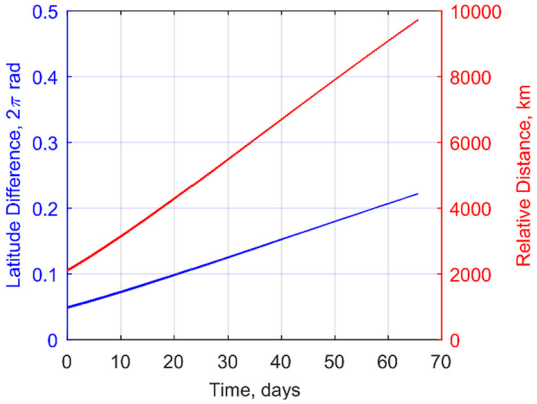

Fig. 10. Time histories of the latitude difference and relative distance for the transfer starting time difference of 2 h ($d_{\text{miss}} = 2096.9$ km).

$$
\begin{aligned}
e_i^{elliF} = & \frac{\left(a_0 - a_{pf}\right)^4 + 10\left(a_0 - a_{pf}\right)^2 \Delta a^2 + \Delta a^4}{3\left(a_0 - a_{pf}\right)^2 \Delta a^2} \\
& - \frac{\left(a_0 - a_{pf}\right)^4 - 6\left(a_0 - a_{pf}\right)^3 \Delta a - 5\left(a_0 - a_{pf}\right)^2 \Delta a^2 - 6\left(a_0 - a_{pf}\right) \Delta a^3 - 2\Delta a^4}{3\left(a_0 - a_{pf}\right)^2 \Delta a^2} e \\
& - \left(\begin{array}{c} \frac{48\left(a_0-a_{pf}\right)^8 + 250\left(a_0-a_{pf}\right)^6 \Delta a^2 + 139\left(a_0-a_{pf}\right)^4 \Delta a^4}{105\left(a_0-a_{pf}\right)^4 \Delta a^4} \\ + \frac{210\left(a_0-a_{pf}\right)^3 \Delta a^5 - 145\left(a_0-a_{pf}\right)^2 \Delta a^6 - 48\Delta a^8}{105\left(a_0-a_{pf}\right)^4 \Delta a^4} \end{array} \right) e^2
\end{aligned} \tag{65}
$$

$$
\begin{aligned}
e_t^{elliE} = & \frac{1}{\left(a_0 - a_{pf}\right) \Delta a} + \frac{\left(a_0 - a_{pf}\right)^4 - 3\left(a_0 - a_{pf}\right) \Delta a^3 - \Delta a^4}{3\left(a_0 - a_{pf}\right)^2 \Delta a^2 \left(\left(a_0 - a_{pf}\right)^2 - \Delta a^2\right)} e \\
& - \left(\begin{array}{c} \frac{22\left(a_0-a_{pf}\right)^8 + 10\left(a_0-a_{pf}\right)^7 \Delta a - 21\left(a_0-a_{pf}\right)^6 \Delta a^2 - 10\left(a_0-a_{pf}\right)^5 \Delta a^3}{30\left(a_0-a_{pf}\right)^3 \Delta a^3 \left(\left(a_0-a_{pf}\right)^2 - \Delta a^2\right)^2} \\ + \frac{58\left(a_0-a_{pf}\right)^4 \Delta a^4 + 20\left(a_0-a_{pf}\right)^3 \Delta a^5 - 51\left(a_0-a_{pf}\right)^2 \Delta a^6 - 20\left(a_0-a_{pf}\right) \Delta a^7 + 22\Delta a^8}{30\left(a_0-a_{pf}\right)^3 \Delta a^3 \left(\left(a_0-a_{pf}\right)^2 - \Delta a^2\right)^2} \end{array} \right) e^2
\end{aligned} \tag{66}
$$

$$
\begin{aligned}
e_i^{elliE} = & -\frac{\left(a_0 - a_{pf}\right)^2 + \Delta a^2}{3\left(a_0 - a_{pf}\right)^2 \Delta a^2} \\
& + \frac{\left(a_0 - a_{pf}\right)^4 - 6\left(a_0 - a_{pf}\right)^3 \Delta a + 3\left(a_0 - a_{pf}\right)^2 \Delta a^2 + 6\left(a_0 - a_{pf}\right) \Delta a^3 + 2\Delta a^4}{3\left(a_0 - a_{pf}\right)^2 \Delta a^2 \left(\left(a_0 - a_{pf}\right)^2 - \Delta a^2\right)} e \\
& + \left(\begin{array}{c} \frac{48\left(a_0-a_{pf}\right)^{10} + 154\left(a_0-a_{pf}\right)^8 \Delta a^2 + 8\left(a_0-a_{pf}\right)^6 \Delta a^4 + 210\left(a_0-a_{pf}\right)^5 \Delta a^5}{105\left(a_0-a_{pf}\right)^4 \Delta a^4 \left(\left(a_0-a_{pf}\right)^2 - \Delta a^2\right)^2} \\ - \frac{97\left(a_0-a_{pf}\right)^4 \Delta a^6 + 210\left(a_0-a_{pf}\right)^3 \Delta a^7 - 49\left(a_0-a_{pf}\right)^2 \Delta a^8 - 48\Delta a^{10}}{105\left(a_0-a_{pf}\right)^4 \Delta a^4 \left(\left(a_0-a_{pf}\right)^2 - \Delta a^2\right)^2} \end{array} \right) e^2
\end{aligned} \tag{67}
$$

Appendix B

This Appendix provides the interpretation on the three cases shown in Fig. 5 (latitude resonance does not happen; latitude resonance happens; satellite-pair miss distance is always given by the relative distance at the first latitude resonance).

If the transfer starting time difference is small, then the latitude difference will be accordingly small over the entire transfer, as the satellites follow an orbital path with the same geometry, such that the latitude resonance won't happen. Fig. 10 presents the time histories of the latitude difference and relative distance for the transfer starting time difference of 2 h. It can be seen that the latitude resonance does not happen.

Once the transfer starting time difference increases to a minimum threshold, the latitude difference will accumulate to be larger than 2π—the latitude resonance happens. Fig. 11 presents the time histories of the latitude difference and relative distance for the transfer starting time difference of 12 h. It can be seen that the satellite-pair miss distance equals to the relative distance at the latitude resonance.

As the transfer starting time difference increases, the latitude difference accumulates faster and faster and the frequency of the latitude difference accordingly increases. Fig. 12 a) and b) present the time histories of the latitude difference and relative distance for the transfer starting time difference of 3 days and 6 days, respectively. The satellite-pair miss distance equals to the relative distance at the first and the second latitude resonance, respectively.

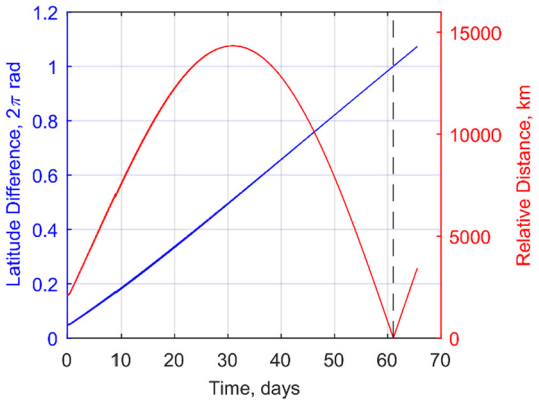

Fig. 11. Time histories of the latitude difference and relative distance for the transfer starting time difference of 12 h ($d_{\text{miss}} = 5.2$ km).

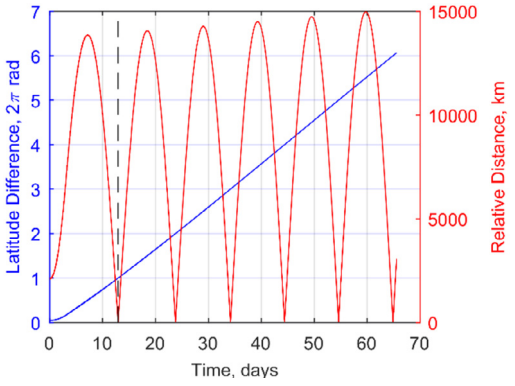

a) Transfer starting time difference of 3 days (d_{miss} = 23.6 km).

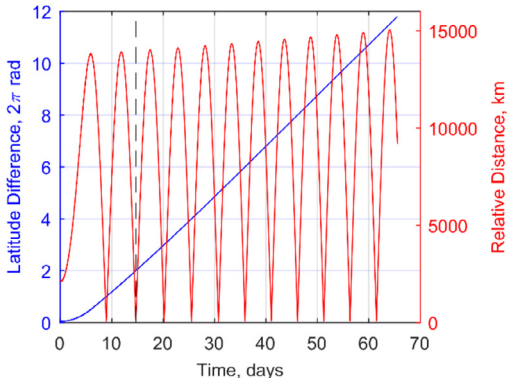

b) Transfer starting time difference of 6 days (d_{miss} = 53.4 km).

Fig. 12. Time histories of the relative distance and latitude difference.

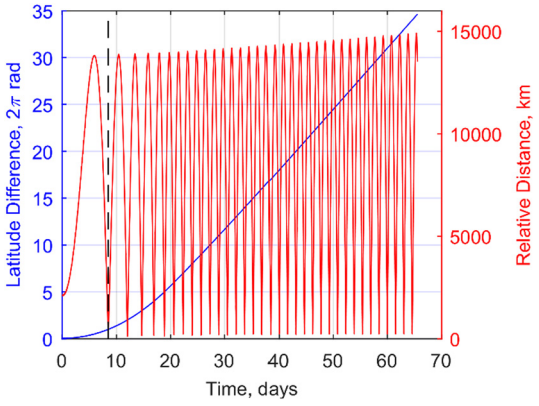

Fig. 13. Time histories of the latitude difference and relative distance for the transfer starting time difference of 20 days ($d_{\text{miss}} = 70.5$ km).

Once the transfer starting time difference increases to the value at which one of the satellites does not start to transfer yet while the other flies by, the satellite-pair miss distance will always be the orbital radius difference at the first fly-by, or the first latitude resonance. Fig. 13 presents the time histories of the latitude difference and relative distance for the transfer starting time difference of 20 days.

Appendix C

Fig. 14 shows the satellite-pair miss distance versus the transfer starting time difference for the satellite pairs with different initial relative phases. The critical transfer starting time difference Δt_0^{safe} and $\Delta t_0^{\text{safest}}$ are highlighted by the blue cross and red asterisk, respectively.

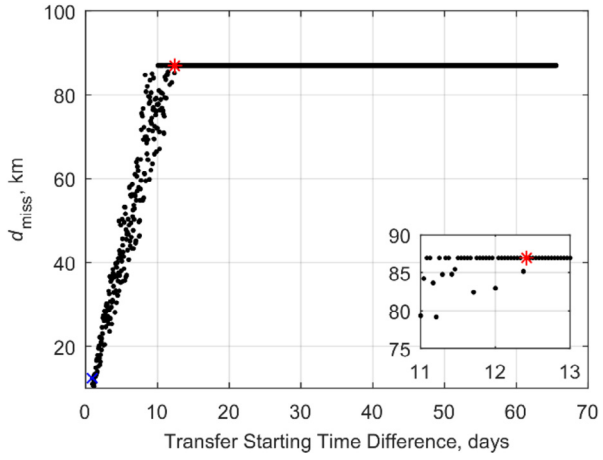

a) $\Delta f_0 = 4\pi/20$ rad

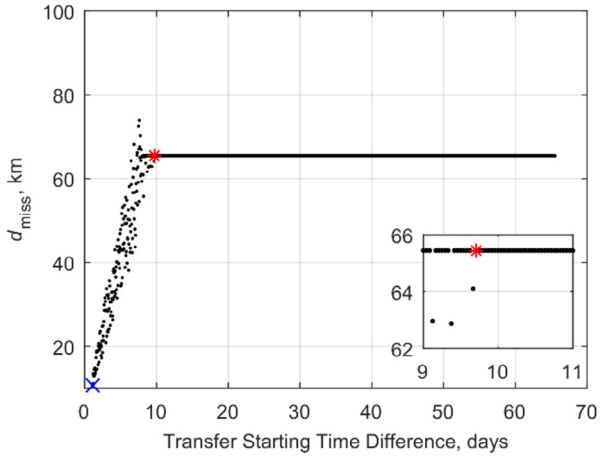

b) $\Delta f_0 = 6\pi/20$ rad

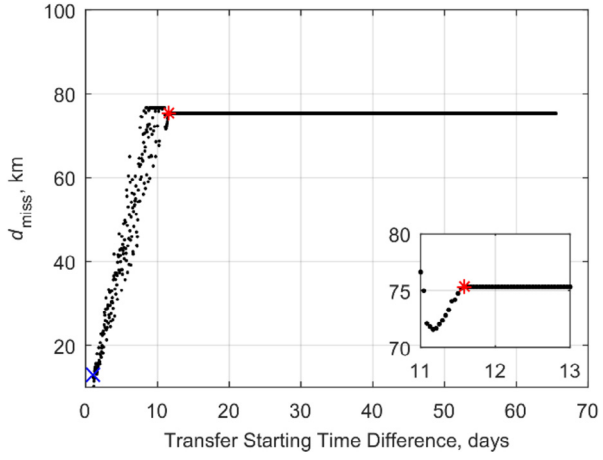

c) $\Delta f_0 = 8\pi/20$ rad

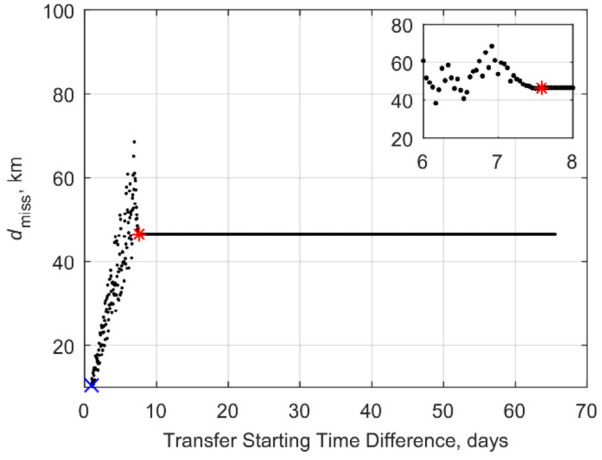

d) $\Delta f_0 = 10\pi/20$ rad

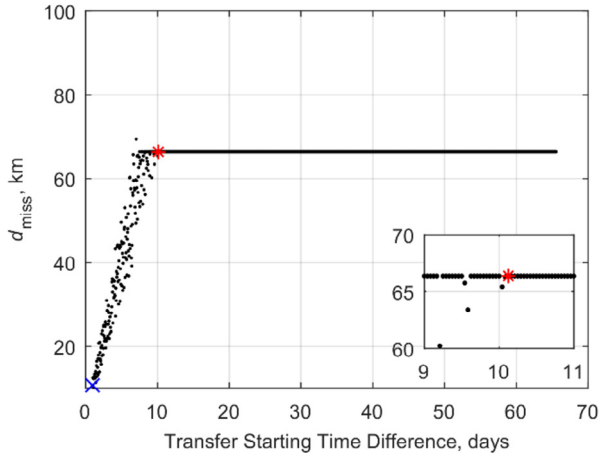

e) $\Delta f_0 = 12\pi/20$ rad

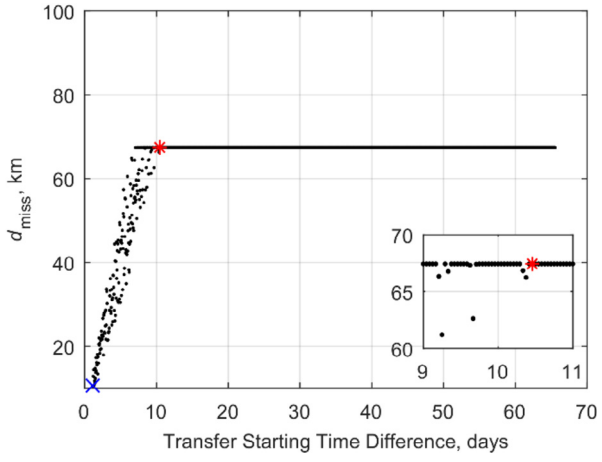

f) $\Delta f_0 = 14\pi/20$ rad

Fig. 14. Satellite-pair miss distance versus transfer starting time difference for different satellite pairs.

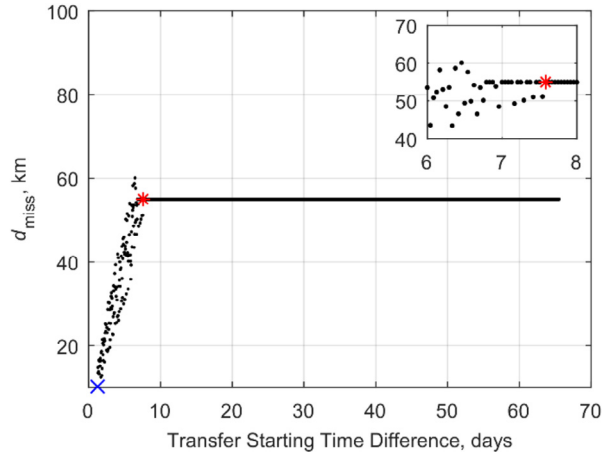

g) $\Delta f_0 = 16\pi/20$ rad

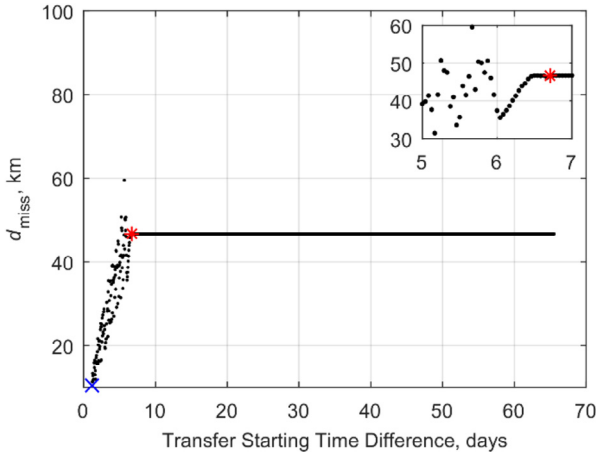

h) $\Delta f_0 = 18\pi/20$ rad

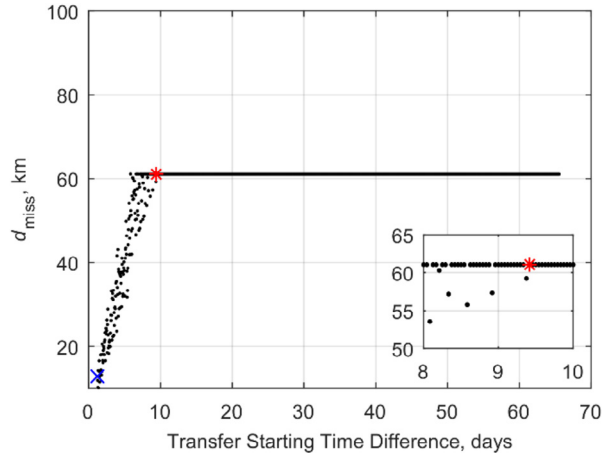

i) $\Delta f_0 = 20\pi/20$ rad

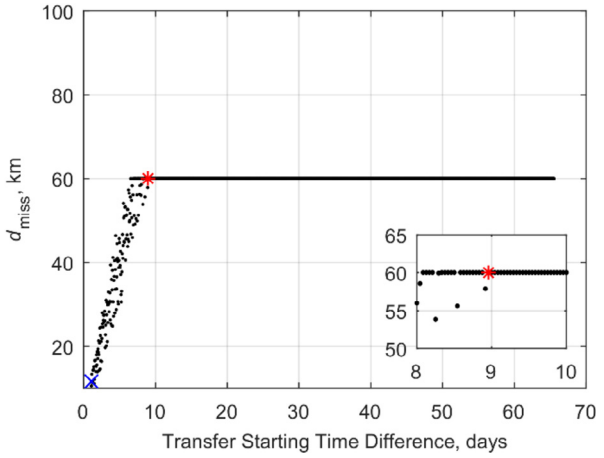

j) $\Delta f_0 = 22\pi/20$ rad

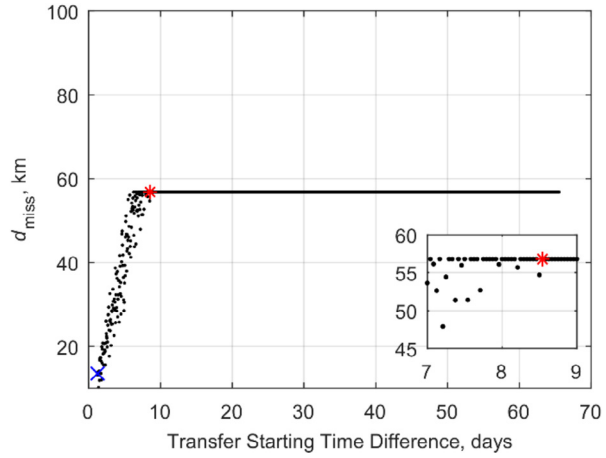

k) $\Delta f_0 = 24\pi/20$ rad

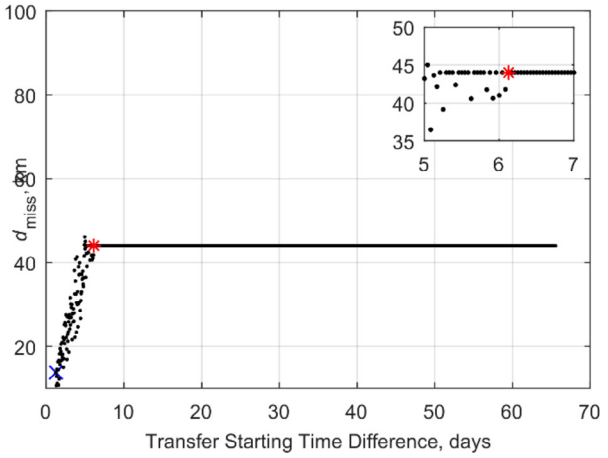

l) $\Delta f_0 = 26\pi/20$ rad

Fig. 14. (*continued*)

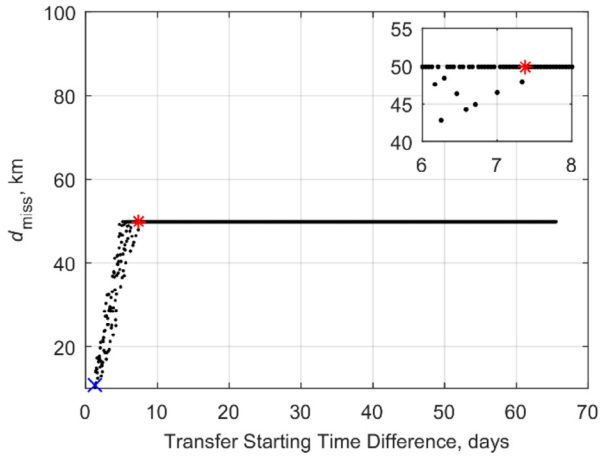

m) $\Delta f_0 = 28\pi/20$ rad

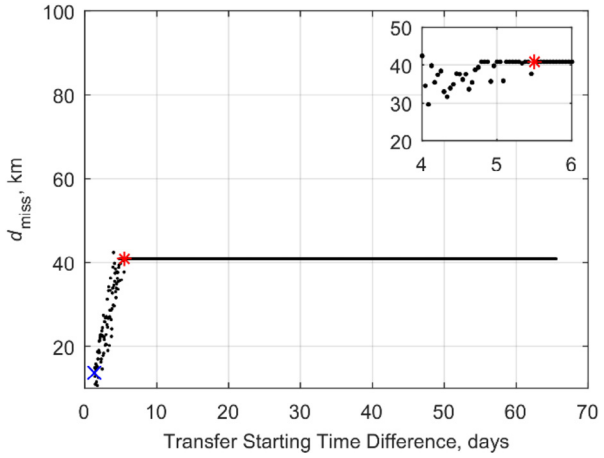

n) $\Delta f_0 = 30\pi/20$ rad

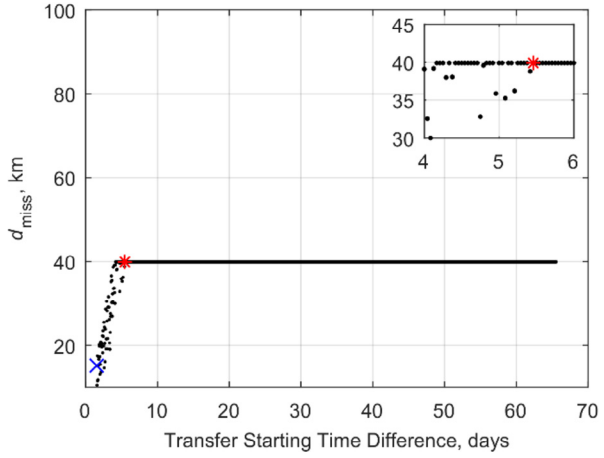

o) $\Delta f_0 = 32\pi/20$ rad

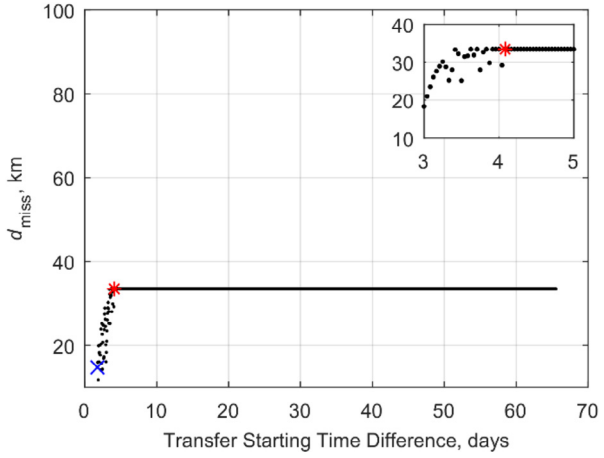

p) $\Delta f_0 = 34\pi/20$ rad

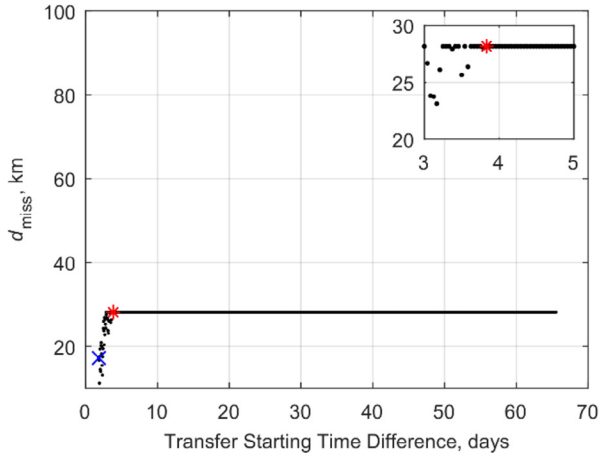

q) $\Delta f_0 = 36\pi/20$ rad

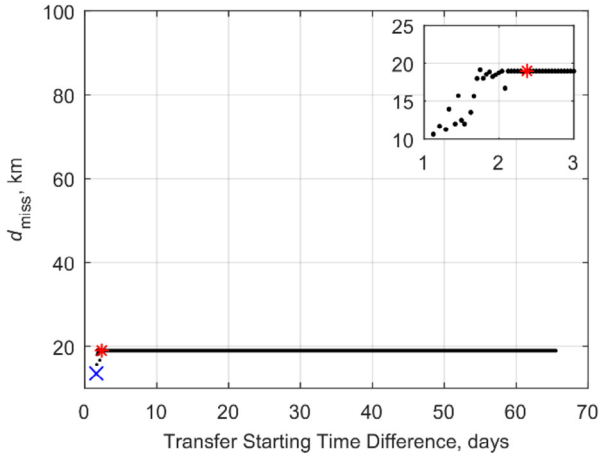

r) $\Delta f_0 = 38\pi/20$ rad

Fig. 14. (*continued*)

References

[1] http://www.oneweb.world/ (Accessed 29 November 2019).
[2] https://www.starlink.com/ (Accessed 29 November 2019).
[3] European Space Agency, End of Life Operations for Disposal of Mega-Constellations, 2016.
[4] European Space Research and Technology Centre, Test Bed for Demonstration of the Safety of Future Telecommunication Constellations, n.d.
[5] D. Ye, M. Shi, Z. Sun, Satellite proximate pursuit-evasion game with different thrust, Aerosp. Sci. Technol. 99 (2020) 105715, https://doi.org/10.1016/j.ast.2020.105715.
[6] J.T. Betts, Very low-thrust trajectory optimization using a direct SQP method, J. Comput. Appl. Math. 120 (2000) 27–40, https://doi.org/10.1016/S0377-0427(00)00301-0.
[7] C.A. Kluever, S.R. Oleson, Direct approach for computing near-optimal low-thrust Earth-orbit transfers, J. Spacecr. Rockets 35 (1998) 509–515, https://doi.org/10.2514/2.3360.
[8] Y. Gao, Near-optimal very low-thrust Earth-orbit transfers and guidance schemes, J. Guid. Control Dyn. 30 (2007) 529–539, https://doi.org/10.2514/1.24836.
[9] Z. Fan, M. Huo, N. Qi, Y. Xu, Z. Song, Fast preliminary design of low-thrust trajectories for multi-asteroid exploration, Aerosp. Sci. Technol. 93 (2019), https://doi.org/10.1016/j.ast.2019.07.028.
[10] A. Ruggiero, P. Pergola, S. Marcuccio, M. Andrenucci, Low-thrust maneuvers for the efficient correction of orbital elements, in: 32nd Int. Electr. Propuls. Conf., Wiesbaden, Germany, 2011.
[11] L. Zhang, B. Xu, M. Li, F. Zhang, Semi-analytical approach for computing near-optimal low-thrust transfers to geosynchronous orbit, Aerosp. Sci. Technol. 55 (2016) 482–493, https://doi.org/10.1016/j.ast.2016.06.022.
[12] M. Di Carlo, L. Ricciardi, M. Vasile, Multi-objective optimisation of constellation deployment using low-thrust propulsion, in: AIAA/AAS Astrodyn. Spec. Conf., Long Beach, California, 2016.
[13] J. Radtke, C. Kebschull, E. Kebschull, Interactions of the space debris environment with mega constellations-using the example of the OneWeb constellation, Acta Astronaut. 131 (2017) 55–68, https://doi.org/10.1016/j.actaastro.2016.11.021.
[14] H.G. Lewis, J. Radtke, J. Beck, B. Bastida Virgili, H. Krag, Self-induced collision risk analysis for large constellations, in: 7th Eur. Conf. Sp. Debris, 2017, https://eprints.soton.ac.uk/id/eprint/414287.
[15] G.L. Somma, H.G. Lewis, C. Colombo, Space debris: analysis of a large constellation at 1200 km altitude, in: 69th Int. Astronaut. Congr., Bremen, Germany, 2018.
[16] K. Lee, H. Park, C. Park, S.Y. Park, Sub-optimal cooperative collision avoidance maneuvers of multiple active spacecraft via discrete-time generating functions, Aerosp. Sci. Technol. 93 (2019) 105298, https://doi.org/10.1016/j.ast.2019.07.031.
[17] R.H. Battin, An Introduction to the Mathematics and Methods of Astrodynamics, American Institute of Aeronautics and Astronautics, Inc., 1999.
[18] J.E. Pollard, Simplified approach for assessment of low-thrust elliptical orbit transfers, in: 25th Int. Electr. Propuls. Conf., Cleveland, Ohio, 1997, pp. 979–986.
[19] A. Spitzer, Near optimal transfer orbit trajectory using electric propulsion, in: Spacefl. Mech., 1995, pp. 1031–1044.
[20] J.A. Kechichian, Orbit raising with low-thrust tangential acceleration in presence of Earth shadow, J. Spacecr. Rockets 35 (1998) 516–525, https://doi.org/10.2514/2.3361.
[21] A. Gaudel, C. Hourtolle, J.F. Goester, M. Ottaviani, De-orbit strategies with low-thrust propulsion, in: Sp. Saf. Is No Accid., Springer, Cham, 2015, pp. 59–68.
[22] M. Vasile, Robust mission design through evidence theory and multiagent collaborative search, Ann. N.Y. Acad. Sci. 1065 (2005) 152–173, https://doi.org/10.1196/annals.1370.024.